Ain Shams Engineering Journal 16 (2025) 103639

Contents lists available at ScienceDirect

Ain Shams Engineering Journal

journal homepage: https://www.sciencedirect.com

Full Length Article

Robust finite-time model reference adaptive control for attitude control of four-rotor unmanned aerial vehicle with disturbances

Syed Awais Ali Shah [a], Shuanghe Yu [a,*], Mohammed El-Meligy [b,c], Haitham A. Mahmoud [d], Nigar Ahmed [e], Aziz Noor [f]

[a] College of Marine Electrical Engineering, Dalian Maritime University, Dalian, 116026, China
[b] Jadara University Research Center, Jadara University, P.O.Box 733, Irbid, Jordan
[c] Applied Science Research Center, Applied Science Private University, Amman, Jordan
[d] Department of Industrial Engineering, College of Engineering, King Saud University, Riyadh 12372, Saudi Arabia
[e] College of Automation, Nanjing University of Aeronautics and Aeronautics, Nanjing, 210016, China
[f] Dalian Key Lab of Marine Micro/Nano Energy and Self-Powered Systems, Marine Engineering College, Dalian Maritime University, Dalian, 116026, China

ARTICLE INFO

Keywords:
Adaptive control
Backstepping
Barrier Lyapunov function
Nonsingular terminal sliding mode control
Disturbance observer

ABSTRACT

This paper presents a new hybrid control framework—Model Reference Adaptive Control with a Barrier Lyapunov Function-based PID Backstepping Nonsingular Terminal Sliding Mode Control (MRA-BLF-PBNTSMC)—for robust attitude control of four-rotor UAVs under disturbances and uncertainties. By integrating a PID-type tracking error formulation within the BLF structure, the proposed method rigorously enforces state constraints while achieving finite-time convergence. A disturbance observer is employed to estimate unknown external disturbances in real time, and dynamic surface control is used to simplify backstepping implementation by avoiding repeated derivative calculations. The control laws are derived using Lyapunov stability theory, guaranteeing finite-time convergence and robustness against model uncertainties. Simulation results show that MRA-BLF-PBNTSMC achieves smoother control input, faster convergence, and reduced steady-state error compared with other methods, while effectively mitigating chattering and singularity issues. These results confirm the method's applicability for UAVs operating in complex environments.

Nomenclature

UAV → Unmanned Aerial Vehicle
MRAC → Model Reference Adaptive Control
BLF → Barrier Lyapunov Function
PID → Proportional-Integral-Derivative
SMC → Sliding Mode Control
TSMC → Terminal Sliding Mode Control
BNTSMC → Backstepping Nonsingular Terminal Sliding Mode Control
PBNTSMC → PID-based Backstepping Nonsingular Terminal Sliding Mode Control
MRA-BLF-PBNTSMC → Model Reference Adaptive BLF-based PID Backstepping Nonsingular Terminal Sliding Mode Control
MRA-BLF-BNTSMC → Model Reference Adaptive BLF-based Backstepping Nonsingular Terminal Sliding Mode Control
MRA-BLF-BSMC → Model Reference Adaptive BLF-based Backstepping Sliding Mode Control
DSC → Dynamic Surface Control
DO → Disturbance Observer
DOF → Degrees of Freedom
Roll → Rotation around the longitudinal axis
Pitch → Rotation around the lateral axis
Yaw → Rotation around the vertical axis
Chattering → High-frequency oscillations in control signals
Singularity → A condition where control signals become undefined or infinite
Finite-time Convergence → Convergence of system states in a finite time interval
State Constraints → Limits placed on system variables
Tracking Error → Difference between actual and reference system outputs

* Corresponding author.
E-mail addresses: awais88pk@outlook.com (S.A.A. Shah), shuanghe@dlmu.edu.cn (S. Yu), mohammedali2000@gmail.com (M. El-Meligy), hmahmoud@ksu.edu.sa (H.A. Mahmoud), Nigar.Ahmed.pk@gmail.com (N. Ahmed), naziz9210@gmail.com (A. Noor).

https://doi.org/10.1016/j.asej.2025.103639
Received 26 December 2024; Received in revised form 20 May 2025; Accepted 10 July 2025

Available online 30 July 2025

1. Introduction

In this modern era, multirotor unmanned aerial vehicles (UAVs or flying robots) are being extensively used in different applications like rescue and search missions, agricultural protection, surveillance, logistics, delivery, tall structures operations at remote areas such as offshore floating wind turbines, and many more applications [1–3]. Beyond their conventional uses, UAVs are revolutionizing a wide range of sectors. They are essential instruments in contemporary culture because of their effectiveness, adaptability, and capacity to function in a variety of settings. The four-rotor UAV or quadrotor UAV is a prominent design of multirotor UAVs [4,5], which contains four rotors assembled on a square body frame with a cross sign pattern, as can be seen in Fig. 1. Because of its efficiency, adaptability, and simplicity, this design is highly valued and potentially used in multiple scenarios. This underactuated model layout has multi-input multi-output (MIMO), which consists of four inputs and six outputs, high coupling effect complexity, and nonlinear dynamics. Therefore, designing the control system for a four-rotor UAV is a difficult challenge.

The uncertainties, unmodeled dynamics, and environmental disturbances have a substantial effect on UAV performance, leading to problems with stability, reduced efficiency, higher energy usage, sensor interference, structural stress, difficulties with control, and navigational errors [6,7]. Normally, the system faces internal or external disturbances. External disturbances are mostly caused by environmental situations that negatively impact the drone's or control system's performance. On the other hand, unmodeled dynamics, noise, and parametric fluctuations brought on by outside disturbances are the sources of internal disturbances. Recently, control engineers' primary goal has been to design precise autopilot systems for UAVs. Disturbance observer-based control (DOBC) is commonly used to mitigate the disturbances from such nonlinear systems [8–10]. Using control inputs and measured outputs, the disturbance observer makes real-time estimations of external disturbances. By estimating these interruptions by the observer's feedback, the controller subsequently improves the stability and robustness of the system.

A control approach called model reference adaptive control (MRAC) uses a reference model to describe the system's desired performance [11]. In order to minimize the difference between the original system's output and the reference model's output, the adaptive controller continually adjusts the control inputs in real time. This ensures that the system stays on the intended trajectory even in the presence of uncertainties or disturbances. This approach is specifically valuable for sustaining robust performance in a variety of operational circumstances and managing dynamic alterations. In [12], a harmful bacterial illness in wheat crops has been determined by using UAV with machine learning and neural network-based model reference intelligent adaptive control. The authors [13] have developed a reference model-based robust control system to improve the utilization of multirotor UAVs in industrial transportation.

Backstepping control methodology ensures system stability by building a Lyapunov function with step-by-step using a recursive procedure. It is mostly useful for nonlinear complex control systems. The authors [14] utilized the backstepping control methodology to design controllers for managing the three operational modes of a biplane quadrotor. Besides this, one of the powerful robust control methods is called sliding mode control (SMC) which applies a discontinuous control signal to nonlinear systems to alter their dynamics and make them follow a predetermined sliding surface. SMC is efficient with handling uncertainties and disturbances, but due to the switches quickly, it frequently causes chattering [15–17]. The impact of integrators in proportional-integral-derivative (PID) control and integral SMC effectively addresses steady-state errors, reduces chattering, and enhances robustness [18–20]. For minimizing chattering, nonsingular terminal sliding mode control (NTSMC) works better. Its beneficial features include smooth control input, finite-time convergence, and avoidance of singularities [21–25].

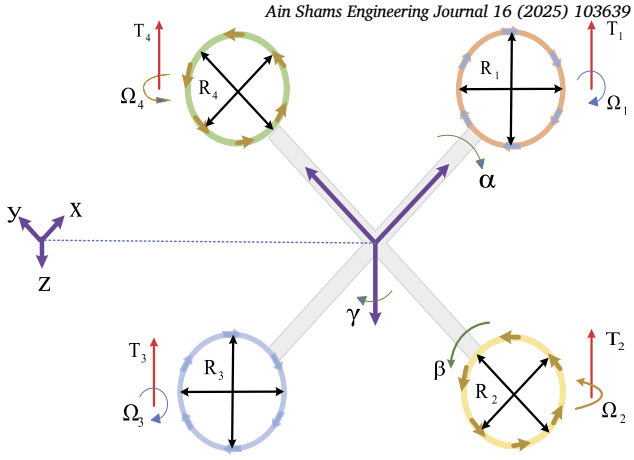

Fig. 1. Schematic of four-rotor UAV.

A four-rotor UAV's attitude angles are normally considered to be between -90° and 90°, which is essential for protecting the mechanical structure, sustaining stability, collecting reliable sensor readings, and simplifying control laws [26–30]. Utilizing the Barrier Lyapunov Function (BLF) when designing a control law guarantees that the constraints stay inside the necessary bounds [31–33]. Four-rotor UAV is an underactuated system, it is challenging to develop an accurate control algorithm under the necessitating consideration of unmodeled dynamics, uncertainties, and disturbances. Some of these problems are addressed separately by different authors using different control strategies [34–38]. To mitigate uncertainties, unmodeled dynamics, disturbances, singularity, and chattering issues, and to pursue accurate attitude tracking purposes, this research work has developed a disturbance observer (DO) based robust control scheme.

This research is motivated by the need for a comprehensive control strategy that can effectively address the aforementioned challenges in real-time flight scenarios. The proposed research targets critical limitations in existing control schemes for quadrotor UAVs operating under dynamic uncertainties and external disturbances. While established techniques such as MRAC, backstepping, and SMC offer robustness, they are often hindered by issues including slow convergence rates, persistent tracking errors, and high control chattering. To overcome these challenges, this study introduces a new hybrid control strategy—PID-based backstepping nonsingular terminal sliding mode control (PBNTSMC). The design synergistically incorporates a Barrier Lyapunov Function to rigorously enforce state constraints, a real-time disturbance observer to compensate for unknown external inputs, and dynamic surface control to simplify derivative computations and improve implementation feasibility. Collectively, these enhancements enable fast and finite-time convergence, strong robustness against disturbances, and smoother control actions, thereby advancing the practical applicability of quadrotor control beyond the capabilities of traditional methods. The key novelties and contributions of this study are summarized as follows:

1. **Robust Hybrid Controller Design:** A new MRA-BLF-PBNTSMC framework is developed by integrating a Barrier Lyapunov Function (BLF) into a PID-based Backstepping Nonsingular Terminal Sliding Mode Control (PBNTSMC) structure within the Model Reference Adaptive Control (MRAC) paradigm to achieve robust attitude control of the UAV.
2. **Disturbance Compensation:** A real-time disturbance observer is introduced to estimate and reject external unknown disturbances, enhancing system robustness.
3. **Reduced Computational Complexity:** Dynamic surface control is utilized to avoid recursive differentiation and improve implementation feasibility.

4. **Numerical Validation:** The proposed control scheme is evaluated through comprehensive simulations. Results show superior tracking performance of roll, pitch, and yaw angles within the defined constraints, improved convergence speed, and reduced chattering when compared to MRA-based BLF-BSMC and MRA-based BLF-BNTSMC controllers.

These enhancements collectively demonstrate improved stability, finite-time convergence, and high tracking accuracy, which make the proposed control law practically viable for UAV operations in uncertain and dynamic environments. The remainder of the paper is organized as follows: Part 2 presents the four-rotor UAV's attitude dynamical model and prerequisites. Part 3 covers the different phases of the DO-based robust control design. Part 4 includes the simulation results and their discussion, and Part 5 provides conclusive remarks.

2. Attitude dynamics and prerequisites for a four-rotor UAV

2.1. Attitude dynamics of a four-rotor UAV

Fig. 1 represents a schematic diagram of a four-rotor UAV. It has four rotors (R_i) directed upward with thrust (T_i) and angular velocity (Ω_i), where i = 1,2,3,4. The attitude roll, pitch, and yaw angles are represented by α, β, and γ along the Cartesian coordinates x, y, and z, respectively. Following [10], the four-rotor UAV attitude model can be represented as a nonlinear system that is: $\dot{X}(t) = g(X, U)$ such as

$$\dot{X}(t) = \begin{bmatrix} \dot{\alpha} \\ v_1\dot{\beta}\dot{\gamma} + v_2\Omega_i\dot{\beta} + v_6U_\alpha \\ \dot{\beta} \\ v_3\dot{\alpha}\dot{\gamma} - v_4\Omega_i\dot{\alpha} + v_7U_\beta \\ \dot{\gamma} \\ v_5\dot{\alpha}\dot{\beta} + v_8U_\gamma \end{bmatrix} \tag{1}$$

where the state vector $X(t) = \begin{bmatrix} \alpha & \dot{\alpha} & \beta & \dot{\beta} & \gamma & \dot{\gamma} \end{bmatrix}^T = \begin{bmatrix} x_a & x_b & x_c & x_d & x_e & x_f \end{bmatrix}^T$. Therefore, Eq. (1) can be rewritten as:

$$\begin{bmatrix} \dot{x}_a \\ \dot{x}_b \\ \dot{x}_c \\ \dot{x}_d \\ \dot{x}_e \\ \dot{x}_f \end{bmatrix} = \begin{bmatrix} x_b \\ v_1x_dx_f + v_2\Omega_ix_d + v_6U_\alpha \\ x_d \\ v_3x_bx_f - v_4\Omega_ix_b + v_7U_\beta \\ x_f \\ v_5x_bx_d + v_8U_\gamma \end{bmatrix} \tag{2}$$

Some of the constant variables are defined as: $v_1 = I_x^{-1}(I_y - I_z)$, $v_2 = I_x^{-1}(J_i)$, $v_3 = I_y^{-1}(I_z - I_x)$, $v_4 = I_y^{-1}(J_i)$, $v_5 = I_z^{-1}(I_x - I_y)$, $v_6 = I_x^{-1}\ell$, $v_7 = I_y^{-1}\ell$, $v_8 = I_z^{-1}$, where ℓ represents the length, J_i is the rotor inertia, and air-frame inertia of the roll, pitch, and yaw are denoted by I_x, I_y, and I_z respectively. While U_α, U_β, and U_γ are the control inputs of roll, pitch, and yaw respectively.

2.2. Prerequisites

Lemma 1. *In nonlinear systems [39], parametric or structured uncertainty can be expressed as:*

$$g^*(x) = \Xi^{*T}\Delta(x) \tag{3}$$

where an unknown vector $\Xi^* = \begin{bmatrix} a_1 & a_2 & \dots & a_p \end{bmatrix}^T \in R^p$ *has constant values and a vector with a bounded basis function is represented by* $\Delta(x) = \begin{bmatrix} b_1(x) & b_2(x) & \dots & b_p(x) \end{bmatrix}^T \in R^p$.

Lemma 2. *Based on Barbalat's lemma [40], as* t *approaches infinity, there exists a differentiable and finite function* g(t) *that shows continuous behavior of* $\dot{g}(t)$*, such that* $\lim_{t\to\infty} \dot{g}(t) = 0$.

Lemma 3. *A dynamic surface control method [41] can eliminate the repeated differentiation in the backstepping virtual law. Its mathematical representation is as follows:*

$$\Theta\dot{\Lambda} + \Lambda = c \tag{4}$$

where Λ *is the first-order filter with having virtual control* c *and time constant* Θ*. The initial condition is assumed that* $\Lambda(0) = c(0)$.

Lemma 4. *Based on the continuous nature of functions [42],* s(x) *is a continuous function that can be restricted by a maximum value* $\bar{s}$*, assuming the initial conditions are in a compact set.*

Assumption 1. *It is assumed that [10] the attitude roll angle* α *and the pitch angle* β *of the Euler-based four-rotor UAV mathematical model are within the interval* $[-\pi/2, \pi/2]$ *to prevent inevitable singularity.*

3. Design of a disturbance observer-based MRA-BLF-PBNTSMC

Firstly, this portion presents the step-by-step design of a disturbance observer-based Model Reference Adaptive PID-based Backstepping Nonsingular Terminal Sliding Mode Control (PBNTSMC) using a Barrier Lyapunov Function (BLF) for the roll dynamics of a four-rotor UAV. Utilizing Eq. (2), the roll model with matched uncertainties and bounded disturbances is expressed as follows:

$$\begin{cases} \dot{x}_a(t) = x_b(t) \\ \dot{x}_b(t) = v_1x_dx_f + v_2\Omega_ix_d + \Xi^T\Delta(\alpha) + v_6U_\alpha + n_\alpha(t) \end{cases} \tag{5}$$

where, according to Lemma 1, the model uncertainties can be represented as $n_1(\delta(\alpha)) = \Xi^T\Delta(\alpha)$ and $n_\alpha(t)$ denotes the matched disturbance.

3.1. Feedback linearization control design

In this step, we will design a feedback linearization control law (U_α) for Eq. (5) as follows:

$$U_\alpha = -v_6^{-1}\left(x_a(t) + x_b(t) + \xi_\alpha - u_\alpha(t)\right) \tag{6}$$

where $\xi_\alpha = v_1x_dx_f + v_2\Omega_ix_d$ and the input $u_\alpha(t)$ needs to be designed. Thus, substituting (6) into (5) results in:

$$\dot{x}_\alpha(t) = A_\alpha x_\alpha(t) + B_\alpha\left(\Xi_\alpha^T\Delta_\alpha(\alpha) + u_\alpha(t)\right) + D_\alpha n_\alpha(t) \tag{7}$$

where $x_\alpha(t) = \begin{bmatrix} x_a(t) & x_b(t) \end{bmatrix}^T$, $A_\alpha = [0 \;\; -1, \; 1 \;\; -1]^T$ $B_\alpha = \begin{bmatrix} 0 & v_\alpha \end{bmatrix}^T$, $D_\alpha = \begin{bmatrix} 0 & 1 \end{bmatrix}^T$, and $v_\alpha = 1$.

3.2. Reference model design

In order to fulfill the criteria of matching and adaptation, the following reference model is selected:

$$\ddot{\theta}_r + 2\iota_r\angle_r\dot{\theta}_r + \angle_r^2\theta_r = v_rr_\alpha(t) \tag{8}$$

where θ_r represents a state variable, and to demonstrate that Eq. (8) is Hurwitz, ι_r and $\angle_r$ are design constants. The constant v_r is associated with the reference input $r_\alpha(t)$. Eq. (8) can now be expressed as follows:

$$\dot{\psi}_r(t) = A_r\psi_r(t) + B_rr_\alpha(t) \tag{9}$$

where $\psi_r(t) = \begin{bmatrix} \psi_1 & \psi_2 \end{bmatrix}^T$, $A_r = \begin{bmatrix} 0 & -\angle_r^2, \; 1 & -2\iota_r\angle_r \end{bmatrix}^T$, and $B_r = \begin{bmatrix} 0 & v_r \end{bmatrix}^T$. The Hurwitz criterion is satisfied by selecting the parameters of A_r such as: $\angle_r = 4$, $v_r = 2$, and $\iota_r = 1/4$.

3.3. Model reference adaptive PBNTSMC design

In this step, the model reference adaptive (MRA) PID-based backstepping nonsingular terminal sliding mode control (MRA-PBNTSMC) input is selected for Eq. (7), as follows:

$$u_\alpha(t) = \hat{H}_\alpha(t)x_\alpha(t) + \hat{h}_1(t)r_\alpha(t) - \hat{h}_2(t)\bar{u}_\alpha(t) - \hat{\Xi}_\alpha^T\Delta_\alpha(\alpha) \tag{10}$$

where adaptive gains are represented as: $\hat{H}_\alpha(t) \in R^{2x2}$, $\hat{h}_1(t) \in R$, and $\hat{h}_2(t) \in R$. The uncertainty estimation and controller are represented by $\hat{\Xi}_\alpha^T\Delta_\alpha(\alpha)$ and $\bar{u}_\alpha(t)$ respectively. Therefore, Eq. (7) can be expressed as:

$$\dot{x}_\alpha(t) = A_\alpha x_\alpha(t) + B_\alpha\bar{u}_\alpha(t) + D_\alpha n_\alpha(t) \tag{11}$$

3.4. Disturbance observer design

According to [10], a standard disturbance observer for Eq. (11) can be designed as follows:

$$\begin{cases} \dot{\hat{n}}_\alpha(t) = \zeta_\alpha D_\alpha\tilde{n}_\alpha(t) \\ \quad\quad = \zeta_\alpha\left(\dot{x}_\alpha - A_\alpha x_\alpha - B_\alpha\bar{u}_\alpha - D_\alpha\hat{n}_\alpha(t)\right) \end{cases} \tag{12}$$

where $\tilde{n}_\alpha(t) = n_\alpha(t) - \hat{n}_\alpha(t)$ and the disturbance observer gain function is represented by ζ_α. The error dynamics of the disturbance observer are obtained as $\dot{\tilde{n}}_\alpha(t) = -\zeta_\alpha D_\alpha\tilde{n}_\alpha^2(t)$. An extra on-board sensor will be required due to the appearance of term $\dot{x}_\alpha$ in Eq. (12). Therefore, by defining an auxiliary variable ∇_α, we can prevent it from this extra burden such as:

$$\nabla_\alpha = \hat{n}_\alpha(t) - \mu_\alpha(x) \tag{13}$$

where the nonlinear design function $\mu_\alpha(x)$ will be used to determine ζ_α, such as: $\zeta_\alpha = \partial\mu_\alpha(x)/\partial x$. An enhanced disturbance observer can be achieved by taking the time derivative of Eq. (13) and further simplifying it, which becomes:

$$\begin{cases} \dot{\nabla}_\alpha = -\zeta_\alpha D_\alpha\nabla_\alpha - \zeta_\alpha\left(A_\alpha x_\alpha + B_\alpha\bar{u}_\alpha + D_\alpha\mu_\alpha(x)\right) \\ \hat{n}_\alpha = \nabla_\alpha + \mu_\alpha(x) \end{cases} \tag{14}$$

A Lyapunov function candidate is selected to determine its error dynamics as follows:

$$V_{\hat{n}_\alpha} = 0.5\tilde{n}_\alpha^2(t) \tag{15}$$

To fulfill the Lyapunov stability criteria, we take the time derivative of Eq. (15) and simplify it further, resulting in:

$$\dot{V}_{\hat{n}_\alpha} = -\zeta_\alpha D_\alpha\tilde{n}_\alpha^2(t) = -\zeta_\alpha D_\alpha\sqrt{2V_{\hat{n}_\alpha}} \tag{16}$$

Hence, the error dynamics of both the standard disturbance observer and the enhanced disturbance observer are stable and identical.

3.5. Backstepping-based model design

In backstepping, we first select the following auxiliary variable:

$$\lambda_1 = x_a(t) - \psi_1 \tag{17}$$

By taking the derivative of Eq. (17), we obtain:

$$\dot{\lambda}_1 = \dot{x}_a(t) - \dot{\psi}_1 = x_b(t) - \psi_2 \tag{18}$$

The Lyapunov function is used in the backstepping method as a design tool; therefore, various issues arise due to taking the derivative of uncertainties, disturbances, and the auxiliary control law. So, this problem can be resolved using Lemma 3. Now we can design an auxiliary feedback control input $c_\alpha(t)$ as follows:

$$c_\alpha(t) = -j_1\lambda_1 + \psi_2 \tag{19}$$

where j_1 is a positive constant. Now, to follow Lemma 3, we can design a filter to resolve the issue of repeated derivatives of the auxiliary feedback control input, such as:

$$\Theta_\alpha\dot{\Lambda}_\alpha + \Lambda_\alpha = c_\alpha \tag{20}$$

where $\Lambda_\alpha(0) = c_\alpha(0)$, $\Theta_\alpha > 0$, and Λ_α represents a filter. Now, we can take $\varpi_\alpha = \Lambda_\alpha - c_\alpha$ and λ_2 as follows:

$$\lambda_2 = x_b(t) - \psi_2 - \Lambda_\alpha \tag{21}$$

After this, we can now take $\dot{\Lambda}_\alpha = -\varpi_\alpha/\Theta_\alpha$ and $x_b(t) = \lambda_2 + \psi_2 + \varpi_\alpha + c_\alpha$. We can rewrite equation (18) using Eq. (19) as follows:

$$\dot{\lambda}_1 = -j_1\lambda_1 + \lambda_2 + \varpi_\alpha + \psi_2 \tag{22}$$

Now, we can take the Lyapunov function candidate in the following manner:

$$V_{\lambda_a} = 0.5(\lambda_1^2 + \varpi_\alpha^2) \tag{23}$$

Applying the derivative to Eq. (23) and simplifying the expression gives us:

$$\dot{V}_{\lambda_a} \le -j_1\lambda_1^2 + (\lambda_2 + \varpi_\alpha + \psi_2)\lambda_1 - (\varpi_\alpha^2/\Theta_\alpha) - K_\alpha(\Im)\varpi_\alpha \tag{24}$$

where a continuous function $K_\alpha(\Im) = K_\alpha(\lambda_1, \lambda_2, \varpi_\alpha, \psi_1, \psi_2) = (\partial c_1\dot{x}_a/\partial x_a) + (\partial c_1\dot{\lambda}_1/\partial\lambda_1)$ fulfills the Lemma 4 criteria. Now, we can simplify it further as follows:

$$\dot{V}_{\lambda_a} \le -(j_1 - 1.5)\lambda_1^2 - \Theta_\alpha^{-1}\varpi_\alpha^2 - 0.5(\bar{K}_\alpha^2 + \lambda_2^2) \tag{25}$$

Hence, $\dot{V}_{\lambda_a} \le 0$ if $j_1 \ge 1.5$. Now, we can write the backstepping-based state-space model as follows:

$$\begin{cases} \dot{\lambda}_1 = -j_1\lambda_1 + \lambda_2 + \varpi_\alpha + \psi_2 \\ \dot{\lambda}_2 = -x_a(t) - x_b(t) + \bar{u}_\alpha(t) + \angle_1^2\psi_1 + 2\imath_1\angle_1\psi_2 \\ \quad -v_\alpha r_\alpha(t) + \varpi_\alpha/\Theta_\alpha \end{cases} \tag{26}$$

3.6. BLF-based PBNTSMC design

To design a BLF-based PBNTSMC, we will select the following sliding mode surface, such as:

$$\Upsilon_\alpha(\lambda_\alpha) = \begin{bmatrix} j_2 & 1 \end{bmatrix}\begin{bmatrix} \lambda_1 + \int\lambda_1 & \lambda_2 + j_4\lambda_2^{j_7} \end{bmatrix}^T \tag{27}$$

where j_2 and j_3 are the positive constants, while $j_4 = 1/j_3$. Similarly, $j_7 = j_5/j_6$ where j_5 and j_6 are positive odd integers that fulfill the criteria $j_6 < j_5 < 2j_6$. Now, select an appropriate Barrier Lyapunov function candidate as follows:

$$V_\alpha(t) = |\Upsilon_\alpha| + 0.5j_8\ln(j_9^2/(j_9^2 - \lambda_1^2)) \tag{28}$$

where j_8 and j_9 are the positive gain constants. Now, taking the time derivative of Eq. (28) and further simplifying will yield:

$$\begin{aligned} \dot{V}_\alpha(t) = \operatorname{sgn}(\Upsilon_\alpha)\big[&G + j_2(j_1\lambda_1 + \lambda_1 + \lambda_2 + \varpi_\alpha + \psi_2) \\ &+ (1 + j_{10}\lambda_2^{j_{11}})\bar{u}_\alpha(t) - L\big] \end{aligned} \tag{29}$$

where $j_{10} = j_5/j_3j_6$, $j_{11} = (j_5 - j_6)/j_6$, $G = (1 + j_{10}\lambda_2^{j_{11}})(-x_a(t) - x_b(t) + n_\alpha(t) + \angle_1^2\psi_1 + 2\imath_1\angle_1\psi_2 - v_\alpha r_\alpha(t) + \varpi_\alpha/\Theta_\alpha) + j_8\lambda_1(j_9^2 - \lambda_1^2)^{-1}(|\Upsilon_\alpha| + (\varpi_\alpha + \psi_2)\operatorname{sgn}(\Upsilon_\alpha))$, and $L = j_8\lambda_1(j_9^2 - \lambda_1^2)^{-1}(j_1\lambda_1 + (j_2\lambda_1 + j_2\int\lambda_1 + j_4\lambda_2^{j_7}))$. Now, we can select the robust control law $\bar{u}_\alpha(t)$ as follows:

$$\bar{u}_\alpha(t) = -\frac{1}{(1 + j_{10}\lambda_2^{j_{11}})}\begin{bmatrix} j_2 & 1 \end{bmatrix} \times \begin{bmatrix} -j_1\lambda_1 + \lambda_2 + \varpi_\alpha + \psi_2 \\ G + \left(j_{12}\left(\frac{\lambda_1}{\sqrt{j_9^2 - \lambda_1^2}} + \sqrt{|2\Upsilon_\alpha|}\right) - L + j_{13}\right)\operatorname{sgn}(\Upsilon_\alpha) \end{bmatrix} \tag{30}$$

where j_{12} and j_{13} are positive gain constants, and the disturbance factor $n_\alpha(t)$ appearing in G is replaced with the estimated disturbance $\hat{n}_\alpha(t)$. Now, substituting Eq. (30) into Eq. (29) and using Young's inequality, we obtain:

$$\dot{V}_\alpha(t) \le -j_{12}\sqrt{2V_\alpha} - j_{13} + 0.5\,\tilde{n}_\alpha^2 \tag{31}$$

Hence, with the proper selection of the switching gains (j_{12}, j_{13}) and the design of the estimated disturbance ($\hat{n}_\alpha(t)$), we can guarantee the Lyapunov finite-time stability of the BLF-based PBNTSMC.

3.7. Adaptive control with adaptive gain design

In this article, we address unmodeled dynamics, matched disturbances, and uncertainties. To prevent the switching gain criteria from being affected by uncertainties in the model, we have introduced adaptive criteria into the proposed controller, which can adapt to the uncertain behavior of the model. For this purpose, we can consider the following uncertain system from Eq. (7), such as:

$$\dot{x}_\alpha(t) = A_\alpha x_\alpha(t) + B_\alpha \left(\Xi_\alpha^T \Delta_\alpha(\alpha) + u_\alpha(t)\right) \tag{32}$$

Let the tracking error be defined as:

$$\perp_\alpha(t) = x_\alpha(t) - \psi_r(t) \tag{33}$$

Substituting $\dot{x}_\alpha(t)$, $\dot{\psi}_r(t)$, and $u_\alpha(t)$ after taking the derivative of Eq. (32) as follows:

$$\begin{aligned}\dot{\perp}_\alpha(t) = &\left(A_\alpha + B_\alpha \hat{H}_\alpha(t)\right) x_\alpha(t) - A_r \psi_r(t) + \left(B_\alpha \hat{h}_1(t) - B_r\right) r_\alpha(t) \\ &+ B_\alpha \tilde{\Xi}^T \Delta(\alpha) - B_\alpha \hat{h}_2(t) \bar{u}_\alpha(t)\end{aligned} \tag{34}$$

The matching conditions according to the model reference control law are expressed as:

$$\begin{cases} A_\alpha + B_\alpha H_\alpha = A_r \\ B_\alpha h_1 = B_r \end{cases} \tag{35}$$

The adaptive errors are defined as:

$$\begin{cases} \tilde{H}_\alpha(t) = H_\alpha - \hat{H}_\alpha(t) \\ \tilde{h}_1(t) = h_1 - \hat{h}_1(t) \\ \tilde{h}_2(t) = h_2 - \hat{h}_2(t) \\ \tilde{\Xi}_\alpha(t) = \Xi_\alpha - \hat{\Xi}_\alpha(t) \end{cases} \tag{36}$$

Substituting the respective values into Eq. (34), we get the following expression:

$$\begin{aligned}\dot{\perp}_\alpha(t) = &A_r \perp_\alpha(t) - B_\alpha \tilde{H}_\alpha(t) x_\alpha(t) - B_\alpha \tilde{h}_1(t) r_\alpha(t) + B_\alpha \tilde{h}_2(t) \bar{u}_\alpha(t) \\ &+ B_\alpha \tilde{\Xi}_\alpha^T \Delta(\alpha)\end{aligned} \tag{37}$$

Now, we can define a Lyapunov function as:

$$\begin{aligned}V\left(\perp_\alpha, \tilde{H}_\alpha, \tilde{h}_1, \tilde{h}_2, \tilde{\Xi}\right) = &\perp_\alpha^T P \perp_\alpha + v_\alpha \left(\tilde{H}_\alpha j_{13a}^{-1} \tilde{H}_\alpha^T + j_{14a}^{-1} \tilde{h}_1^2\right. \\ &\left. + j_{14b}^{-1} \tilde{h}_2^2 + \tilde{\Xi}_\alpha^T j_{13b}^{-1} \tilde{\Xi}_\alpha\right)\end{aligned} \tag{38}$$

Here, the positive-definite matrices are defined as: $j_{13a} = j_{13a}^T \in R^{2x2}$, $j_{13b} = j_{13b}^T \in R^{2x2}$, while j_{14a} and j_{14b} are the positive adaptive gains. Now, defining the matrices $P = P^T > 0 \in R^{2x2}$ and $Q = Q^T \in R^{2x2}$ where

$$-Q = PA_r + A_r^T P \tag{39}$$

For simplicity, the derivative of Eq. (38) is defined as: $\dot{V}(\dagger) = \dot{V}\left(\perp_\alpha, \tilde{H}_\alpha, \tilde{h}_1, \tilde{h}_2, \tilde{\Xi}\right)$. Substitute Eq. (37) into $\dot{V}(\dagger)$ as follows:

$$\begin{aligned}\dot{V}(\dagger) = &\perp_\alpha^T (PA_r + A_r^T P) \perp_\alpha + 2 \perp_\alpha^T P B_\alpha \left(-\tilde{H}_\alpha x_\alpha(t) + \tilde{h}_2(t) \bar{u}_\alpha\right. \\ &- \tilde{h}_1(t) r_\alpha(t) + \tilde{\Xi}^T \Delta(\alpha)\Big) + v_\alpha \left(2 \tilde{H}_\alpha j_{13a}^{-1} \dot{\tilde{H}}_\alpha^T + 2 j_{14a}^{-1} \tilde{h}_1 \dot{\tilde{h}}_1\right. \\ &\left. + 2 j_{14b}^{-1} \tilde{h}_2 \dot{\tilde{h}}_2 + 2 \tilde{\Xi}_\alpha^T j_{13b}^{-1} \dot{\tilde{\Xi}}_\alpha\right)\end{aligned} \tag{40}$$

The parameters of matrix P are further defined as: $P = \begin{bmatrix} \bar{P}_1 & \bar{P}_2 \end{bmatrix}$, where $\bar{P}_1 = \begin{bmatrix} j_{1a} & j_{2a} \end{bmatrix}^T$ and $\bar{P}_2 = \begin{bmatrix} j_{1b} & j_{2b} \end{bmatrix}^T$. Now, we can derive the following relation:

$$2 \perp_\alpha^T P B_\alpha = 2 \perp_\alpha^T \bar{P}_2 v_\alpha \in R \tag{41}$$

Now, by using Eq. (39) and Eq. (41), we can further simplify $\dot{V}(\dagger)$ as follows:

$$\begin{aligned}\dot{V}(\dagger) = &-\perp_\alpha^T Q \perp_\alpha + 2 v_\alpha \tilde{H}_\alpha \left(-x_\alpha(t) \perp_\alpha^T \bar{P}_2 + j_{13a}^{-1} \dot{\tilde{H}}_\alpha^T{}_\alpha(t)\right) \\ &+ 2 v_\alpha \tilde{h}_1 \left(-r_\alpha(t) \perp_\alpha^T \bar{P}_2 + j_{14a}^{-1} \dot{\tilde{h}}_1\right) + 2 v_\alpha \tilde{h}_2 \left(\bar{u}_\alpha \perp_\alpha^T \bar{P}_2\right. \\ &\left. + j_{14b}^{-1} \dot{\tilde{h}}_2\right) + 2 v_\alpha \tilde{\Xi}^T \left(\Delta(\alpha) \perp_\alpha^T \bar{P}_2 + j_{13b}^{-1} \dot{\tilde{\Xi}}_\alpha\right)\end{aligned} \tag{42}$$

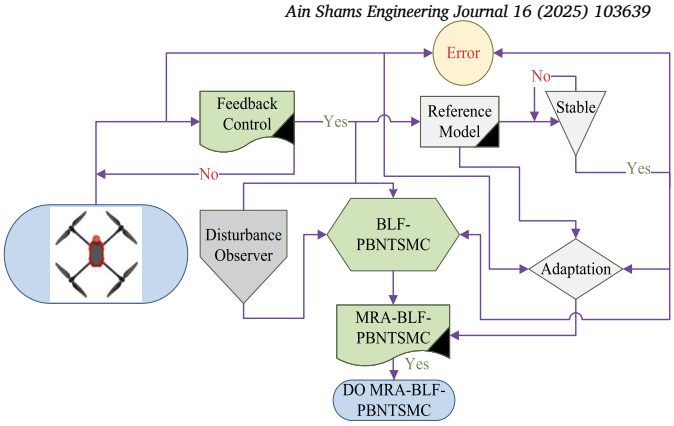

Fig. 2. Flow diagram of the DO-based MRA-BLF-PBNTSMC for the attitude control of a four-rotor UAV.

From this, we can design adaptive gain laws as follows:

$$\begin{cases} \dot{\tilde{H}}_\alpha^T = j_{13a} x_\alpha(t) \perp_\alpha^T \bar{P}_2 \\ \dot{\tilde{h}}_1 = j_{14a} r_\alpha(t) \perp_\alpha^T \bar{P}_2 \\ \dot{\tilde{h}}_2 = -j_{14b} \bar{u}_\alpha \perp_\alpha^T \bar{P}_2 \\ \dot{\tilde{\Xi}}_\alpha = -j_{13b} \Delta(\alpha) \perp_\alpha^T \bar{P}_2 \end{cases} \tag{43}$$

Substituting the adaptive gain laws into Eq. (42) yields:

$$\dot{V}(\dagger) = -\perp_\alpha^T Q \perp_\alpha \le -E_{min}(Q) \left\| \perp_\alpha \right\|_2^2 \le 0 \tag{44}$$

where the minimum eigenvalue of the matrix Q is represented by $E_{min}(Q)$. Hence, we can conclude that the adaptive gains $\hat{H}_\alpha$, $\hat{h}_1$, $\hat{h}_2$, and $\hat{\Xi}_\alpha$ in the proposed adaptive control law $u_\alpha(t)$ are bounded and stable. We can further write the expression as:

$$\begin{aligned}\lim_{t \to \infty} V(\dagger) &= V\left(\perp_\alpha, \tilde{H}_\alpha, \tilde{h}_1, \tilde{h}_2, \tilde{\Xi}\right) \\ &= \lim_{t \to \infty} V\left(\perp_{\alpha_0}, \tilde{H}_{\alpha_0}, \tilde{h}_{1_0}, \tilde{h}_{2_0}, \tilde{\Xi}_0\right) - E_{min}(Q) \left\| \perp_\alpha \right\|_2^2\end{aligned} \tag{45}$$

where the initial condition of the Lyapunov candidate function is represented as: $V(\dagger_0) = V\left(\perp_{\alpha_0}, \tilde{H}_{\alpha_0}, \tilde{h}_{1_0}, \tilde{h}_{2_0}, \tilde{\Xi}_0\right)$, and Fig. 2 is the flow diagram of the DO-based MRA-BLF-PBNTSMC for the attitude control of a four-rotor UAV. In a compact form, the DO-based MRA-BLF-PBNTSMC can be represented in the theorem below.

Theorem 1. *The following DO-based MRA-BLF-PBNTSMC mitigates uncertainties, unmodeled dynamics, and disturbances in a four-rotor UAV, guaranteeing the tracking of attitude angles.*

Attitude DO-based MRA-BLF-PBNTSMC:

$$\begin{cases} U_\phi = -v_{6\phi}^{-1} \left(x_{a\phi}(t) + x_{b\phi}(t) + \xi_\phi - u_\phi(t)\right) \\ u_\phi(t) = \hat{H}_\phi(t) x_\phi(t) + \hat{h}_{1\phi}(t) r_\phi(t) - \hat{h}_{2\phi}(t) \bar{u}_\phi(t) - \hat{\Xi}_\phi^T \Delta_\phi(\phi) \\ \bar{u}_\phi(t) = -\frac{1}{(1 + j_{10\phi} \lambda_{2\phi}^{j11\phi})} \left(j_{2\phi}(-j_{1\phi} \lambda_{1\phi} + \lambda_{2\phi} + \varpi_\phi + \psi_{2\phi}) + G_\phi\right. \\ \qquad \left. + j_{12\phi} \mathrm{sgn}(\Upsilon_\phi) \left(\lambda_{1\phi} (j_{9\phi}^2 - \lambda_{1\phi}^2)^{-0.5} + \sqrt{\left|2\Upsilon_\phi\right|}\right)\right. \\ \qquad \left. + j_{13\phi} \mathrm{sgn}(\Upsilon_\phi)\right) \end{cases} \tag{46}$$

Adaptive Gains:

$$\begin{cases} \dot{\tilde{H}}_\phi^T = j_{13a\phi} x_\phi(t) \perp_\phi^T \bar{P}_{2\phi} \\ \dot{\tilde{h}}_{1\phi} = j_{14a\phi} r_\phi(t) \perp_\phi^T \bar{P}_{2\phi} \\ \dot{\tilde{h}}_{2\phi} = -j_{14b\phi} \bar{u}_\phi \perp_\phi^T \bar{P}_{2\phi} \\ \dot{\tilde{\Xi}}_\phi = -j_{13b\phi} \Delta(\phi) \perp_\phi^T \bar{P}_{2\phi} \end{cases} \tag{47}$$

Disturbance Observer:

$$\begin{cases} \dot{\nabla}_\phi = -\zeta_\phi D_\phi \nabla_\phi - \zeta_\phi \left(A_\phi x_\phi + B_\phi \bar{u}_\phi + D_\phi \mu_\phi(x)\right) \\ \hat{n}_\phi = \nabla_\phi + \mu_\phi(x) \end{cases} \tag{48}$$

where ϕ represents attitude angles (α, β, γ). Furthermore, the gain parameter of the disturbance observer ζ_ϕ and the switching law gains (j_{12}, j_{13}) have to fulfill their respective conditions.

Proof. Consider a Lyapunov function in the following manner:

$$V_{T\phi} = \sum_{\phi=\alpha}^{\gamma} \left(V_\phi(t) + V_{\hat{n}\phi}(t) + V_{\varpi\phi}(t) + V\left(\perp_\phi, \tilde{H}_\phi, \tilde{h}_{1\phi}, \tilde{h}_{2\phi}, \tilde{\Xi}_\phi\right)\right) \tag{49}$$

where $V_{\hat{n}_\phi} = 0.5\tilde{n}_\phi^2(t)$, $V\left(\perp_\phi, \tilde{H}_\phi, \tilde{h}_{1\phi}, \tilde{h}_{2\phi}, \tilde{\Xi}_\phi\right) = \perp_\phi^T P_\phi \perp_\phi + v_\phi\left(\tilde{H}_\phi j_{13\phi}^{-1} \tilde{H}_\phi^T + j_{14\phi}^{-1} \tilde{h}_{1\phi}^2 + j_{14b\phi}^{-1} \tilde{h}_{2\phi}^2 + \tilde{\Xi}_\phi^T j_{13b\phi}^{-1} \tilde{\Xi}_\phi\right)$, $V_\phi(t) = \left|\Upsilon_\phi\right| + 0.5 j_{8\phi} \ln(j_{9\phi}^2/(j_{9\phi}^2 - \lambda_{1\phi}^2))$, and $V_{\varpi\phi}(t) = 0.5\varpi_\phi^2$. Now, taking the time derivative of Eq. (49) gives us:

$$\begin{aligned} \dot{V}_{T\phi} = \sum_{\phi=\alpha}^{\gamma} & \left(\operatorname{sgn}\left(\Upsilon_\phi\right)\right)\left[j_{2\phi}\left(j_{1\phi}\lambda_{1\phi} + \lambda_{1\phi} + \lambda_{2\phi} + \varpi_\phi + \psi_{2\phi}\right)\right. \\ & \left(1 + j_{10\phi}\lambda_{2\phi}^{j_{11\phi}}\right)\bar{u}_\phi(t) + G_\phi\Big] - L_\phi + v_\phi\left(2\tilde{H}_\phi j_{13a\phi}^{-1}\dot{\tilde{H}}_\phi^T\right. \\ & + 2j_{14a\phi}^{-1}\tilde{h}_{1\phi}\dot{\tilde{h}}_{1\phi} + 2j_{14b\phi}^{-1}\tilde{h}_{2\phi}\dot{\tilde{h}}_{2\phi} + 2\tilde{\Xi}_\phi^T j_{13b\phi}^{-1}\dot{\tilde{\Xi}}_\phi\Big) \\ & \left. + \tilde{n}_\phi\dot{\tilde{n}}_\phi + \varpi_\phi\dot{\varpi}_\phi + \dot{\perp}_\phi^T P_\phi \perp_\phi + \perp_\phi^T P_\phi \dot{\perp}_\phi\right) \end{aligned} \tag{50}$$

Further simplifying Eq. (50) by using the Young's inequality, it becomes:

$$\begin{aligned} \dot{V}_{T\phi} \le \sum_{\phi=\alpha}^{\gamma} & \left(-j_{12\phi}\sqrt{2V_\phi} - j_{13\phi} + 0.5\tilde{n}_\phi^2 - L_\phi - \hbar_\phi\varpi_\phi^2\right. \\ & \left. -\zeta_\phi D_\phi\sqrt{2V_{\hat{n}_\phi}} - 0.5\bar{K}_\phi^2 - E_{\min}(Q)_\phi\left\|\perp_\phi\right\|_2^2\right) \end{aligned} \tag{51}$$

where $\hbar_\phi = 0.5 + 1/\Theta_\phi > 0$, $\bar{K}_\phi \ge K_\phi(\Im)$, and $K_\phi(\Im)$ is a continuous function. Hence, with the proper selection of the switching gains ($j_{12\phi}$, $j_{13\phi}$) and the design of the estimated disturbance ($\hat{n}_\phi(t)$), we can guarantee the Lyapunov finite-time stability of the DO-based PBNTSMC, which completes the proof. □

Algorithm 1 outlines the pseudocode for attitude control using the disturbance observer-based MRA-BLF-PBNTSMC strategy for a four-rotor UAV.

Algorithm 1 DO-based MRA-BLF-PBNTSMC for Four-Rotor UAV Attitude Control.

Initialize: System parameters υ_i, $j_{\phi i}$, $j_{i\phi}$, ζ_ϕ, Θ_ϕ, controller gains
Set initial states $X(t) = [\alpha, \dot{\alpha}, \beta, \dot{\beta}, \gamma, \dot{\gamma}]^\top$
Define desired trajectory and reference model
while system is operating **do**
  Compute UAV attitude dynamics:
    $\dot{X}(t) = g(X, U)$
  Compute tracking errors:
    $e_\phi = \phi - \phi_{\text{ref}}$
    $\dot{e}_\phi = \dot{\phi} - \dot{\phi}_{\text{ref}}$
  Compute sliding variable using BLF:
    $\Upsilon_\phi = \text{BLF}(e_\phi, \dot{e}_\phi)$
  Update disturbance observer:
    $\dot{\nabla}_\phi = -\zeta_\phi D_\phi \nabla_\phi - \zeta_\phi(A_\phi x_\phi + B_\phi \bar{u}_\phi + D_\phi \mu_\phi(x))$
    $\hat{n}_\phi = \nabla_\phi + \mu_\phi(x)$
  Compute auxiliary control input:
    $\bar{u}_\phi = \text{BLF-PBNTSMC\_Sliding\_Law}(\Upsilon_\phi, \lambda_{i\phi}, j_{i\phi})$
  Compute adaptive control law:
    $u_\phi(t) = \hat{H}_\phi x_\phi + \hat{h}_{1\phi} r_\phi - \hat{h}_{2\phi}\bar{u}_\phi - \hat{\Xi}_\phi^\top \Delta_\phi(\phi)$
    $U_\phi = -v_{6\phi}^{-1}(x_{a\phi} + x_{b\phi} + \xi_\phi - u_\phi)$
  Update adaptive parameters:
    $\dot{\hat{H}}_\phi^\top = j_{13a\phi} x_\phi \theta_\phi^\top \bar{P}_{2\phi}$
    $\dot{\hat{h}}_{1\phi} = j_{14a\phi} r_\phi \theta_\phi^\top \bar{P}_{2\phi}$
    $\dot{\hat{h}}_{2\phi} = -j_{14b\phi}\bar{u}_\phi \theta_\phi^\top \bar{P}_{2\phi}$
    $\dot{\hat{\Xi}}_\phi = -j_{13b\phi}\Delta(\phi)\theta_\phi^\top \bar{P}_{2\phi}$
end while

Table 1
Parameters of the four-rotor UAV.

Parameter	Value	Description
I_x	4.856×10^{-3} kg m^2	Roll airframe inertia
I_y	4.856×10^{-3} kg m^2	Pitch airframe inertia
I_z	8.801×10^{-3} kg m^2	Roll airframe inertia
Ω_i	2.980×10^{-6}	Thrust coefficient
J_i	1.140×10^{-7}	Drag coefficient
g	9.81m/s^2	Gravity of earth
l	0.225m	Distance
m	0.468kg	Mass

Table 2
Observer, controller, and adaptive gains for MRA-BLF-PBNTSMC.

ϕ:	α	β	γ
ζ_ϕ	70	70	70
$j_{\phi 1}$	1	1	1
Θ_ϕ	0.001	0.001	0.001
$j_{\phi 2}$	1	1	1
$j_{\phi 3}$	10	10	10
$j_{\phi 5}/j_{\phi 6}$	7/5	7/5	7/5
$j_{\phi 13}$	100	100	100
$j_{13a\phi}$	[1 0; 0 1]	[1 0; 0 1]	[1 0; 0 1]
$j_{14a\phi}$	50	50	50
$\bar{P}_{2\phi}$	$[50 \quad 50]^T$	$[50 \quad 50]^T$	$[50 \quad 50]^T$

4. Simulation results and discussion

This part presents the simulations of attitude tracking of four-rotor UAV under disturbances, which are obtained by using MATLAB/Simulink. The four-rotor UAV design data is taken from [10] and given in Table 1. The roll model simulation using the design parameters of observer, controller, and adaptive gains for MRA-BLF-PBNTSMC are shown in Table 2. Furthermore, to verify the efficiency and validity of proposed control algorithm (MRA-BLF-PBNTSMC) is compared with two other control laws (MRA-BLF-BNTSMC, MRA-BLF-BSMC).

The simulation outcomes for roll, pitch, and yaw tracking are illustrated in Figs. 3–5. These figures present a comparative analysis of three control strategies: MRA-BLF-PBNTSMC, MRA-BLF-BNTSMC, and MRA-BLF-BSMC. In each plot, the purple line denotes the barrier limits imposed on the respective attitude angles (0.5 rad, 0.4 rad, and 0.3 rad), while the corresponding tracking errors are also depicted. All controllers successfully guide the system to track the desired reference angles (0.3 rad, 0.25 rad, and 0.2 rad) within the predefined constraints. It is evident that all three controllers achieve nearly identical steady-state responses after 4.5 seconds. However, the MRA-BLF-PBNTSMC approach demonstrates superior performance by attaining significantly lower steady-state errors on the order of 10^{-5} for roll, pitch, and yaw, respectively. The effectiveness of all compared controllers is attributed to the inclusion of the Barrier Lyapunov Function, which strictly enforces state constraints and enhances overall stability and tracking precision. Among them, the proposed control method demonstrates improved accuracy, faster convergence, and robust tracking under the imposed BLF criteria. A comparative performance index for all three MRA-BLF-based robust controllers is presented in Table 3. In case of MRA-BLF-BSMC law the standard sliding mode surface is selected as: $\Upsilon_\phi\left(\lambda_\phi\right) = j_2\lambda_1 + j_{2\phi}\lambda_2$, where gain constant $j_{2\phi} = 2$. Furthermore all the remaining gain parameters of all three control laws are same as shown in Table 2.

To rigorously evaluate the effectiveness of the proposed control scheme, a disturbance observer is employed to estimate nonlinear disturbances acting on the roll dynamics. The observer demonstrates accurate tracking of external perturbations, thereby enabling the controller to robustly reject uncertainties and maintain system stability, as illustrated in Fig. 6. The disturbance modeled in this simulation is defined as follows:

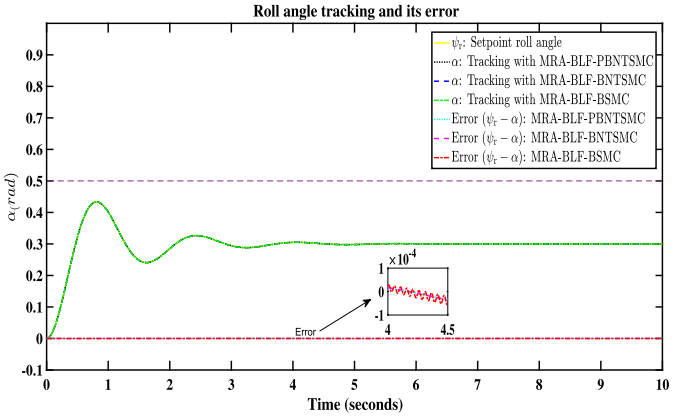

Fig. 3. Performance of roll angle tracking.

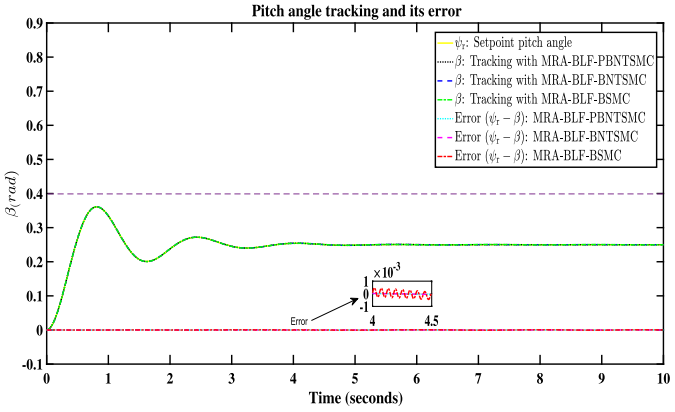

Fig. 4. Performance of pitch angle tracking.

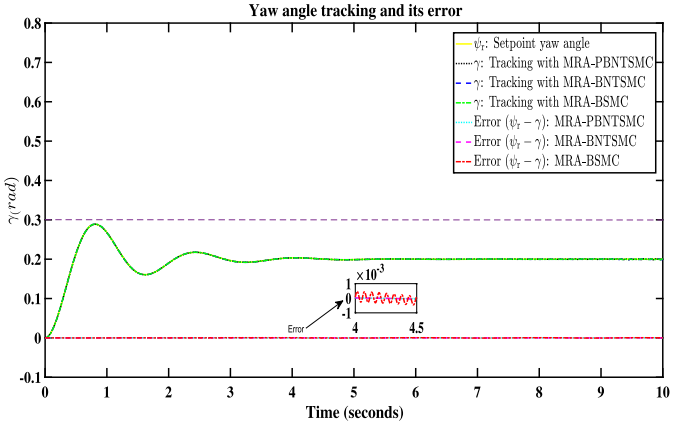

Fig. 5. Performance of yaw angle tracking.

$$n_\alpha(t) = A \cdot \sin\left(2\pi\left(f_0 t + \frac{(f_1 - f_0)}{2T}t^2\right)\right) \tag{52}$$

Here, A denotes the disturbance amplitude, f_0 is the initial frequency, f_1 represents the final frequency at the sweep time T, and t is the time variable. This chirp signal formulation enables comprehensive disturbance modeling across a broad frequency range, effectively simulating real-world conditions such as turbulent wind, structural vibrations, or aerodynamic irregularities typically encountered by UAVs.

In Fig. 6, two scenarios are depicted: part (a) evaluates the controller under a low-amplitude, low-frequency disturbance signal, while part (b) examines performance under a high-amplitude, high-frequency disturbance. The simulation results confirm that the proposed approach

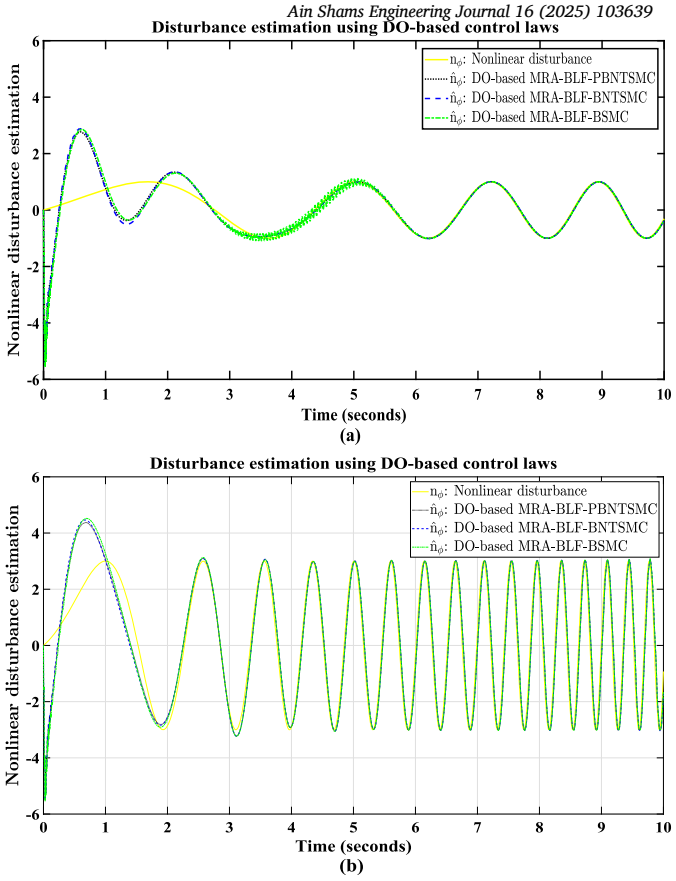

Fig. 6. Nonlinear disturbance estimation.

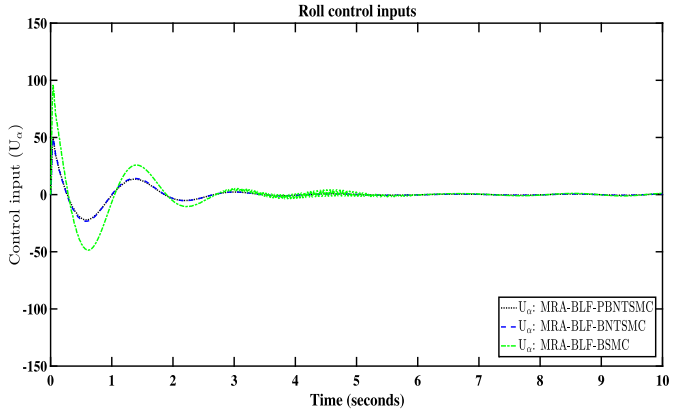

Fig. 7. Control inputs for the roll angle.

retains finite-time convergence and robust tracking in both mild and extreme disturbance conditions.

Fig. 7 illustrates the control input responses corresponding to the roll angle trajectory tracking under external disturbances. Among the three control strategies evaluated, the MRA-BLF-BSMC scheme exhibits noticeably higher control effort and more pronounced chattering behavior compared to the proposed MRA-BLF-PBNTSMC. This highlights the improved smoothness and efficiency of the control signal achieved through the integration of PID feedback and dynamic surface control. Additionally, it is observed that the control responses of MRA-BLF-PBNTSMC and MRA-BLF-BNTSMC remain closely aligned across the simulation, indicating comparable performance in terms of control input behavior. The adaptive gains by using the algorithm of the proposed MRA-BLF-PBNTSMC for obtaining desired roll angle tracking and mitigating the unwanted disturbances are shown in Fig. 8. It can be clearly seen from

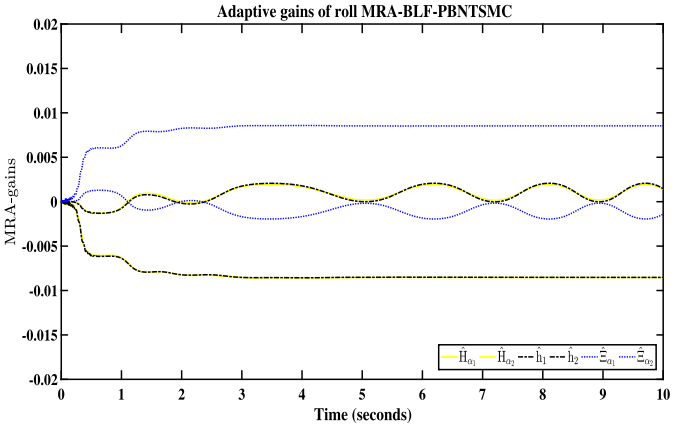

Fig. 8. MRA-BLF-PBNTSMC-based adaptive gains for roll angle.

Table 3
Performance indices for MRA-BLF-based robust controllers.

Parameters	MRA-BLF PBNTSMC	MRA-BLF BNTSMC	MRA-BLF BSMC
RMSE(α)	$4.725e^{-05}$	$5.719e^{-05}$	$6.957e^{-05}$
RMSE(β)	$6.712e^{-05}$	$8.754e^{-05}$	$7.31e^{-04}$
RMSE(γ)	$5.27e^{-05}$	$6.926e^{-05}$	$8.771e^{-05}$
Control Effort	Excellent	V.Good	Good
Robustness	Yes	Yes	Yes
Stability	Finite-Time	Finite-Time	Asymptotically

all the simulation figures for roll model that the performance of the proposed MRA-BLF-PBNTSMC is better than MRA-BLF-BNTSMC and MRA-BLF-BSMC. On the other hand, the overall performance of MRA-BLF-BSMC is not as efficient as MRA-BLF-PBNTSMC and MRA-BLF-BNTSMC due to the selection of sliding surfaces. Furthermore, the performance of these control techniques is almost the same for pitch and yaw models.

5. Conclusion

This paper has introduced a robust hybrid control approach for attitude tracking of a four-rotor unmanned aerial vehicle (UAV) under the influence of external bounded disturbances and modeling uncertainties. The proposed method integrates model reference adaptive control with a Barrier Lyapunov function-based PID backstepping nonsingular terminal sliding mode control (MRA-BLF-PBNTSMC) framework to ensure smooth and precise trajectory tracking.

Simulation-based evaluations have demonstrated that the proposed control law achieves finite-time convergence, suppresses chattering and singularity issues, and maintains tracking accuracy even under rapidly changing and high-amplitude disturbances. Comparative analysis with two other schemes—MRA-BLF-BNTSMC and MRA-BLF-BSMC— further validates the superior performance of the proposed approach in terms of precision, convergence speed, and robustness.

Beyond theoretical and simulation benefits, the control strategy shows promise for real-world UAV applications where strong robustness is critical. Such scenarios include aggressive flight maneuvers, disturbance-prone environments, and missions requiring high-accuracy performance such as aerial inspection, package delivery, and autonomous navigation in cluttered or dynamic settings.

Based on Lyapunov-based stability analysis and disturbance observer integration, the proposed MRA-BLF-PBNTSMC control framework has been shown to be a reliable and effective solution for UAV attitude control tasks involving external disturbances.

Future work will focus on extending the control design to the full 6-DOF dynamics of a four-rotor UAV, including both attitude and translational control. Additionally, real-time implementation and validation of the proposed MRA-BLF-PBNTSMC controller on a hardware-in-the-loop (HIL) testbed or actual UAV platform will be pursued to evaluate its practical feasibility and performance in real-world flight scenarios.

CRediT authorship contribution statement

Syed Awais Ali Shah: Writing – review & editing, Writing – original draft, Methodology. **Shuanghe Yu:** Writing – review & editing, Supervision, Conceptualization. **Mohammed El-Meligy:** Visualization, Investigation, Formal analysis. **Haitham A. Mahmoud:** Visualization, Project administration, Funding acquisition, Formal analysis. **Nigar Ahmed:** Writing – review & editing, Validation, Conceptualization. **Aziz Noor:** Validation, Software, Methodology.

Declaration of competing interest

The authors declare that they have no known competing financial interests or personal relationships that could have appeared to influence the work reported in this paper.

Acknowledgement

The authors extend their appreciation to King Saud University, Saudi Arabia for funding this work through Ongoing Research Funding Program, (ORF-2025-1006), King Saud University, Riyadh, Saudi Arabia.

References

[1] Zhang S, He Y, Gu Y, He Y, Wang H, Wang H, et al. Uav based defect detection and fault diagnosis for static and rotating wind turbine blade: a review. Nondestruct Test Eval 2025;40(4):1691–729.
[2] Labbadi M, Chatri C, Khenfri F. Fixed-time controller for altitude/yaw control of mini-drone based on nonsingular terminal sliding mode: real-time implementation with uncertainties. IFAC J Syst Control 2024;29:100278.
[3] Mobayen S, El-Sousy FF, Alattas KA, Mofid O, Fekih A, Rojsiraphisal T. Adaptive fast-reaching nonsingular terminal sliding mode tracking control for quadrotor uavs subject to model uncertainties and external disturbances. Ain Shams Eng J 2023;14(8):102059.
[4] Liu L, Wu Y, Fu G, Zhou C. An improved four-rotor uav autonomous navigation multisensor fusion depth learning. Wirel Commun Mob Comput 2022;2022(1):2701359.
[5] Ahmed N, Er MJ, Shah SAA. Reduced-order observer based trajectory tracking control of quadrotor subject to noises and disturbances. Int J Control Autom Syst 2025;23(3):860–8.
[6] Ahmed N, Bhatia Ak, Ali Shah SA. Robust active disturbance attenuation control of an uncertain quadrotor. Int J Intell Unmanned Syst 2022;10(4):346–62.
[7] Bhatia AK, Jiang J, Kumar A, Shah SAA, Rohra A, ZiYang Z. Adaptive preview control with deck motion compensation for autonomous carrier landing of an aircraft. Int J Adapt Control Signal Process 2021;35(5):769–85.
[8] Wang L, Sun W, Pei H. Nonlinear disturbance observer-based geometric attitude fault-tolerant control of quadrotors. Int J Syst Sci 2024;55(11):2337–48.
[9] Xie T, Xian B, Gu X, Hu J, Liu M. Disturbance observer-based fixed-time tracking control for a tilt trirotor unmanned aerial vehicle. IEEE Trans Ind Electron 2023;71(4):3894–903.
[10] Ahmed N, Raza A, Shah SAA, Khan R. Robust composite-disturbance observer based flight control of quadrotor attitude. J Intell Robot Syst 2021;103(1):11.
[11] Gong S, Xu Z, Cheng L, Huang X. Self-organizing model reference adaptive control for aircraft with enhanced persistent excitation. Aerosp Sci Technol 2024;145:108875.
[12] Menebo M, Negash L, Shiferaw D. Neural network based model reference adaptive control of quadrotor uav for precision agriculture. In: Pan African conference on artificial intelligence. Springer; 2023. p. 171–93.
[13] Wang Q, Wang W, Suzuki S, Namiki A, Liu H, Li Z. Design and implementation of uav velocity controller based on reference model sliding mode control. Drones 2023;7(2):130.
[14] Dalwadi N, Deb D, Muyeen S. Observer based rotor failure compensation for biplane quadrotor with slung load. Ain Shams Eng J 2022;13(6):101748.
[15] Huang T, Gao X, Li T. Adaptive fuzzy attitude sliding mode control for a quadrotor unmanned aerial vehicle. Int J Fuzzy Syst 2024;26(2):686–701.
[16] Baek J, Kang M. A synthesized sliding-mode control for attitude trajectory tracking of quadrotor uav systems. IEEE/ASME Trans Mechatron 2023;28(4):2189–99.
[17] Rahimpour R, Sepestanaki MA, Mobayen S, Mokhtare Z, Fekih A, Assawinchaichote W, et al. An lmi adaptive-barrier function global sliding mode control of uncertain nonlinear systems with input saturation. Ain Shams Eng J 2024;15(2):102460.
[18] Kazemi MH, Tarighi R. Pid-based attitude control of quadrotor using robust pole assignment and lpv modeling. Int J Dyn Control 2024:1–13.

[19] Shah SAA, Gao B, Ahmed N, Liu C. Advanced robust control techniques for the stabilization of translational oscillator with rotational actuator based barge-type ofwt. Proc Inst Mech Eng, Part M, J Eng Marit Environ 2021;235(2):327–43.
[20] Eltayeb A, Rahmat MF, Basri MAM, Eltoum MM, Mahmoud MS. Integral adaptive sliding mode control for quadcopter uav under variable payload and disturbance. IEEE Access 2022;10:94754–64.
[21] Shah SAA, Gao B, Bhatia AK, Liu C, Rauf A. Anti-vibration control design for tora based barge-type offshore floating wind turbine using extended order high gain observer. Eng Comput 2022;39(7):2705–32.
[22] Rauf A, Zafran M, Khan MSA, Khan A, Shah SAA. Non-singular terminal sliding mode control of converter-fed dc motor system with mismatched disturbance compensation. Int J Model Identif Control 2021;39(4):285–92.
[23] Shah SAA, Gao B, Ahmed N, Liu C, Rauf A. Disturbance observer-based sliding mode control of tora system for floating wind turbines. In: 2019 IEEE 9th annual international conference on CYBER technology in automation, control, and intelligent systems (CYBER). IEEE; 2019. p. 418–23.
[24] Shah SAA, Malik FM, Raza A, Khan R, Ahmed N. Sampled data gyroscope stabilization of two degree of freedom platform. In: 2016 13th international bhurban conference on applied sciences and technology (IBCAST). IEEE; 2016. p. 251–5.
[25] Anwar J, Malik FM. Performance of non-linear observers for closed loop terminal sliding mode control of quadrotor uav. In: 2017 14th international bhurban conference on applied sciences and technology (IBCAST). IEEE; 2017. p. 244–52.
[26] Aslam MS, Bilal H. Modeling a Takagi-Sugeno (ts) fuzzy for unmanned aircraft vehicle using fuzzy controller. Ain Shams Eng J 2024;15(10):102984.
[27] Morchid A, Et-taibi B, Oughannou Z, El Alami R, Qjidaa H, Jamil MO, et al. Iot-enabled smart agriculture for improving water management: a smart irrigation control using embedded systems and server-sent events. Sci Afr 2025;27:e02527.
[28] Morchid A, Jebabra R, Qjidaa H, El Alami R, Jamil MO. Agri-tech innovations for sustainability: a fire detection system based on mqtt broker and iot to improve environmental risk management. Results Eng 2024;24:103683.
[29] Morchid A, Oughannou Z, El Alami R, Qjidaa H, Jamil MO, Khalid HM. Integrated Internet of things (iot) solutions for early fire detection in smart agriculture. Results Eng 2024;24:103392.
[30] Morchid A, Jebabra R, Alami RE, Charqi M, Boukili B. Smart agriculture for sustainability: the implementation of smart irrigation using real-time embedded system technology. In: 2024 4th international conference on innovative research in applied science, engineering and technology (IRASET). IEEE; 2024. p. 1–6.
[31] Liu B, Wang Y, Sepestanaki MA, Pouzesh M, Mobayen S, Rouhani SH, et al. Event-trigger-based adaptive barrier function higher-order global sliding mode control technique for quadrotor uavs. IEEE Trans Aerosp Electron Syst 2024.
[32] Habibi H, Safaei A, Voos H, Darouach M, Sanchez-Lopez JL. Safe navigation of a quadrotor uav with uncertain dynamics and guaranteed collision avoidance using barrier Lyapunov function. Aerosp Sci Technol 2023;132:108064.
[33] Shah SAA, Gao B, Ahmad I, Ullah H, Ahmed N, Saeed A. Adaptive backstepping integral sliding mode control for 5dof barge-type ofwt under output constraint. J Mar Sci Eng 2023;11(3):492.
[34] Han Q, Liu Z, Su H, Liu X. Filter-based adaptive backstepping attitude control for multi-rotor uavs with parametric uncertainty, external disturbance and input saturation. Nonlinear Dyn 2024;112(20):18293–310.
[35] Hu Y, Miao Z, Wang Y, Lin J, Lin Q. Uncertainty and disturbance estimator-based geometry tracking control for quadrotors without linear velocity measurements. Asian J Control 2024;26(2):858–72.
[36] Ahmed N, Ali Shah SA. Adaptive output-feedback robust active disturbance rejection control for uncertain quadrotor with unknown disturbances. Eng Comput 2022;39(4):1473–91.
[37] Liu C, Yu C, Gao B, Ali Shah SA, Tapus A. Towards a balancing safety against performance approach in human–robot co-manipulation for door-closing emergencies. Complex Intell Syst 2022;8(4):2859–71.
[38] Liu C, Gao B, Zhao J, Shah SAA. Orbitally stabilizing control for the underactuated translational oscillator with rotational actuator system: design and experimentation. Proc Inst Mech Eng, Part I, J Syst Control Eng 2019;233(5):491–500.
[39] Nguyen NT, Nguyen NT. Model-reference adaptive control. Springer; 2018.
[40] Slotine J-JE, Li W, et al. Applied nonlinear control, vol. 199. Englewood Cliffs, NJ: Prentice Hall; 1991.
[41] Chen M, Tao G, Jiang B. Dynamic surface control using neural networks for a class of uncertain nonlinear systems with input saturation. IEEE Trans Neural Netw Learn Syst 2014;26(9):2086–97.
[42] Wang D, Huang J. Neural network-based adaptive dynamic surface control for a class of uncertain nonlinear systems in strict-feedback form. IEEE Trans Neural Netw 2005;16(1):195–202.

Syed Awais Ali Shah received a B.S. degree in electronic engineering from COMSATS University, Abbottabad, Pakistan, in 2011, and an M.S. degree in electrical engineering with a specialization in control systems from the National University of Science and Technology (NUST), Islamabad, Pakistan, in 2014. He completed his Ph.D. in electrical engineering at Southeast University, Nanjing, China, in 2023, and is currently a postdoctoral researcher at Dalian Maritime University, Dalian, China. His primary research interests include sampled-data control, anti-vibration control, observer design, and robust control strategies for underactuated mechanical systems.